Local Turbulence Model for Predicting Circulation Rates in Bubble Columns

Karl G. Anderson, Richard G. Rice
Department of Chemical Engineering
Louisiana State University
Baton Rouge, LA 70803

When a gas is sparged into a bubble column, the gas fraction is measurably higher at the center of the column than at the wall. The resulting radial density gradient induces a buoyancy driven circulation, with upflow in the core and downflow in the outer annulus. A reliable first principle to predict elementary fluid flow patterns has eluded scientists, in spite of numerous recent efforts, notably by: Ueyama and Miyauchi (1979); Riquarts (1982); Walter and Blanch (1983); Yang et al. (1986); and Ulbrecht et al. (1985).

This work departs from the cited turbulent gas-liquid models but has similarities to the recent work of Clark et al. (1987). To account for the voidage driving force, we apportion the two-phase flow field into two zones with ϵ in the core and ϵ^* in the annulus, such that $\epsilon^* < \epsilon$. Second, and more importantly, the turbulent stress tensor (Reynolds stress) is taken to be locally varying. The classical turbulence theories of von Kármán and Prandtl are invoked for the two respective zones.

In the present work, complete analytical solutions for time-averaged velocity profiles are derived, in contrast to the numerical solution obtained by Clark et al. (1987). In addition, material and energy balances allow the core voidage (ϵ) and dimensionless inversion position (δ) to be computed directly for known gas rates. The predicted velocity profiles compare quite favorably to the velocity measurements of Hills (1974). Moreover, the new, unified theory shows, for the first time, how increasing molecular viscosity affects circulation rate.

Derivation of Velocity Profile

The voidage distribution is treated simply as a two-zone function, with a higher voidage (ϵ) in the upflowing core and a lower voidage (ϵ^*) in the buffer zone. This approach also has the flexibility for allowing different bubble sizes, since large, faster rising bubbles in the core impart momentum to slower bubbles, driving them into the annular region. Further, the thin laminar boundary layer at the column wall is considered free from bubbles, since a finite bubble has a very limited degree of freedom to reside near the wall. Thus, there exists three basic zones: core, buffer, and clear laminar wall layer.

For steady state conditions, the equations of motion for each zone may be written as suggested by Rietema (1982). For the core, these are:

$$(1-\epsilon)\rho_c U_c \frac{\partial U_c}{\partial z} = -(1-\epsilon)\nabla \cdot R_c - (1-\epsilon)\nabla p - (1-\epsilon)\rho_c g + F_s \quad (1)$$

$$\epsilon\rho_d U_d \frac{\partial U_d}{\partial z} = -\epsilon\nabla \cdot R_c - \epsilon\nabla p - \epsilon\rho_d g - F_s \quad (2)$$

where R_c refers to the Reynolds stress and F_s to the so-called slip force.

Taking the phase densities to be constant and adding Eqs. 1 and 2, noting that $\rho_c \gg \rho_d$, an integration using the symmetry condition $R_c(0) = 0$, yields:

$$R_c = \left[-\frac{dp}{dz} - \rho_c g(1-\epsilon)\right] r/2 = \beta\xi \quad (0 \le r \le b \quad \text{or} \quad 0 \le \xi \le \delta) \quad (3)$$

The von Kármán model for Reynolds stress is then introduced:

$$R_c = \rho_c \kappa^2 \left(-\frac{\partial U_c}{\partial \xi}\right)^4 \Big/ \left(\frac{\partial^2 U_c}{\partial \xi^2} - \frac{1}{\xi}\frac{\partial U_c}{\partial \xi}\right)^2 = \beta\xi \quad (0 \le \xi \le \delta) \quad (4)$$

to yield the velocity gradient:

$$-\frac{dU_c}{d\xi} = \frac{3}{2\Gamma}\frac{\xi}{\alpha^3 - \xi^{3/2}} \quad (5)$$

where α is denoted as the second von Kármán parameter. Since

Correspondence concerning this paper should be sent to Richard G. Rice.

in the core $(-\partial U_c/d\xi) > 0$, it is necessary that

$$\alpha > \sqrt{\delta} \tag{6}$$

Equation 5 may be integrated with the condition $U_c(\delta) = 0$, to give:

$$U_c = \frac{3}{\Gamma}(\sqrt{\xi} - \sqrt{\delta}) + \frac{\alpha}{2\Gamma}\ln\left[\frac{(\alpha - \sqrt{\xi})^2(\alpha^2 + \alpha\sqrt{\delta} + \delta)}{(\alpha - \sqrt{\delta})^2(\alpha^2 + \alpha\sqrt{\xi} + \xi)}\right] + \frac{\alpha\sqrt{3}}{\Gamma}\left[\tan^{-1}\left(\frac{2\sqrt{\delta} + \alpha}{\alpha\sqrt{3}}\right) - \tan^{-1}\left(\frac{2\sqrt{\xi} + \alpha}{\alpha\sqrt{3}}\right)\right] \quad (0 \le \xi \le \delta) \tag{7}$$

A discontinuity at the boundary is avoided by requiring that $\alpha \neq \sqrt{\delta}$.

Proceeding in the same manner for the buffer zone gives:

$$R_c^* = \beta^*(\lambda^2/\xi - \xi) \quad (\delta \le \xi \le \lambda) \tag{8}$$

where the stress continuity condition $R_c(\delta) = R_c^*(\delta)$ has been invoked and λ is defined by $R_c^*(\lambda) = 0$, so that

$$\lambda^2 = \delta^2(\epsilon - \epsilon^*)/[(1 - \epsilon^*) - p'] \tag{9}$$

This denotes the position of maximum downflow velocity $|U^*_{w\max}|$.

Owing to the similarities between the von Kármán and Prandtl models and the ease with which the two may be linked, Prandtl's mixing length theory was chosen to represent the Reynolds stress in the buffer zone. Also, it is reasoned that the buffer and the clear laminar zones sustain the main effects of a higher molecular viscosity, so that:

$$R_c^* = \frac{\mu_c}{R}\left(-\frac{\partial U_w^*}{\partial \xi}\right) + \rho_c l^{*2}\left(-\frac{\partial U_w^*}{\partial \xi}\right)^2 \tag{10}$$

Taking the dimensionless mixing length (l^*) to be constant in this thin region allows Eqs. 8 and 10 to be combined to yield for the buffer zone:

$$-\frac{\partial U_w^*}{\partial \xi} = \frac{-\mu_c}{2\rho_c R l^{*2}} + \sqrt{\left(\frac{\mu_c}{2\rho_c R l^{*2}}\right)^2 + \frac{\beta^*}{\rho_c l^{*2}}\left(\frac{\lambda^2}{\xi} - \xi\right)} \quad (\delta \le \xi \le \lambda) \tag{11}$$

insuring that $\partial U_w^*/\partial \xi = 0$ at $\xi = \lambda$. Equation 11 may be integrated with the condition $U_w^*(\lambda) = U_w(\lambda)$, coupling buffer and wall zones, to obtain:

$$\frac{U_w^*}{|U^*_{w\max}|} = -1 - \frac{1}{2}U_\mu\lambda + U_\mu\xi - \frac{2}{3}U_t\sqrt{\xi}\sqrt{\lambda^2 + N_t^2\lambda\xi - \xi^2} + \frac{4}{3}\lambda^{3/2}U_t g_t[F(\psi_\lambda, k_+) - F(\psi_\xi, k_+)] + \frac{2}{3}\lambda^{3/2}U_t N_t^2\frac{g_t b_t^2}{k_-^2}\{[E(\psi_\lambda, k_+) - E(\psi_\xi, k_+)] - k_-^2[F(\psi_\lambda, k_+) - F(\psi_\xi, k_+)] - k_+^2(sn[F(\psi_\lambda, k_+)]cn[F(\psi_\lambda, k_+)]/dn[F(\psi_\lambda, k_+)] - sn[F(\psi_\xi, k_+)]cn[F(\psi_\xi, k_+)]/dn[F(\psi_\xi, k_+)])\} \tag{12}$$

the functions of which are defined in the notation section. We note that elliptic integrals arise naturally in the analysis (Byrd and Friedman, 1954). The argument for the several elliptic integrals, ψ, is given by:

$$\psi_\xi = \sin^{-1}\sqrt{\frac{2\xi}{\xi + [\lambda + \xi(N_t^2/2)]/\sqrt{(N_t^2/2)^2 + 1}}} \tag{13}$$

Equation 13 simplifies considerably for low viscosity liquids, $(N_t \to 0)$. At the wall, the momentum equations reduce to

$$\tau_w = \frac{\rho_c g R}{2}[1 - p']\left[\frac{\lambda^2}{\xi} - \xi\right] \quad (\lambda \le \xi \le 1) \tag{14}$$

Existence of bubbles in the wall region can be accounted for by replacing $(p' - 1)$ with $(p' - 1 + \epsilon^*)$. When integrated, using the no-slip condition $U_w(1) = 0$ for a Newtonian fluid $(\tau_w = -\mu_c\partial U_w/\partial r)$, Eq. 14 yields:

$$U_w = -\frac{\rho_c g R^2}{4\mu_c}[1 - p'][1 - \xi^2 + \lambda^2 \ln \xi^2] \quad (\lambda \le \xi \le 1) \tag{15}$$

The maximum velocity occurs when $\xi = \lambda$, which we have denoted as $|U^*_{w\max}|$.

The inversion point was defined by $U_c(\delta) = 0$, but this condition has yet to be applied to the buffer zone. Coupling requires $U_w^*(\delta) = 0$; hence Eq. 12 with $\xi = \delta$ may be used to find the appropriate value of λ. When λ is known in terms of ϵ and δ, Eq. 9 yields a direct computation of dimensionless pressure gradient, p'.

To insure a smooth transition from the core to the buffer zone, a continuity condition is applied at the inversion point such that:

$$\frac{dU_c}{d\xi} = \frac{dU_w^*}{d\xi} \quad \text{at} \quad \xi = \delta \tag{16}$$

which, when combined with stress continuity $R_c(\delta) = R_c^*(\delta)$, becomes a kinematic condition requiring equality of effective viscosity at the inversion point δ. Combining Eqs. 5 and 11 defines the buffer zone mixing length (l^*) in terms of the second

von Kármán parameter (α) to be

$$l^* = \frac{2}{3\Gamma}\sqrt{\frac{\beta^*}{\rho_c}}\left[\left(\frac{\alpha}{\sqrt{\delta}}\right)^3 - 1\right] \cdot \sqrt{\lambda^2 - \delta^2\left(1 + \frac{3\mu_c}{2\beta^*\Gamma R\delta^{3/2}}\frac{1}{[(\alpha/\sqrt{\delta})^3 - 1]}\right)} \quad (17)$$

The connection to molecular viscosity is obvious.

Derivation of the Macroscopic Balances

With the velocity profile established, it is necessary to determine two essential quantities: δ (inversion point) and ϵ (core voidage). All other quantities are defined in terms of these essential variables. To find δ and ϵ requires two linearly independent equations. These equations will be the batch conservation relation and the overall energy dissipation rate.

For no net liquid flow (batch), conservation requires upflow equal to downflow

$$Q_c + Q_w^* + Q_w = 0 \quad (18)$$

where Q_c, Q_w^*, and Q_w are the volumetric flowrates in the core, buffer, and laminar layer respectively. These flowrates are determined by integrating the respective velocity profiles (Appendix I).

It is interesting to note that if equal areas for flow are allocated, then $\pi R^2\delta^2 = \pi R^2(1 - \delta^2)$, predicting $\delta = 1/\sqrt{2} = 0.707$. This simple approximation is very close to the so-called universal value of 0.715 deduced by Yang et al. (1986) for inviscid liquids.

The second linearly independent equation connecting δ and ϵ is obtained by equating the rate of energy input to the rate of energy dissipation. Energy is dissipated mainly by two mechanisms in tall columns: mechanical energy dissipation owing to the overall velocity profile, and dissipation in flow around bubbles, so that

$$E_g = E_v + E_b \quad (19)$$

For a uniform pressure, energy input is given by:

$$E_g = Q_d\left(-\frac{dp}{dz}\right)H - \rho_d g H Q_d \simeq Q_d\rho_c g H p' \quad (20)$$

The total dissipation owing to the velocity profiles is partitioned over the three zones:

$$E_v = E_{vc} + E_{vw}^* + E_{vw} \quad (21)$$

For the laminar wall layer, dissipation is computed using:

$$E_{vw} = 2\pi HR\int_\lambda^1\left(-\tau_w\frac{dU_w}{d\xi}\right)\xi\, d\xi \quad (22)$$

Integration by parts yields:

$$E_{vw} = Q_w\rho_c g H[p' - 1] \quad (23)$$

Similarly, for the core and buffer zones respectively,

$$E_{vc} = Q_c\rho_c g H[p' - (1 - \epsilon)] \quad (24)$$

$$E_{vw}^* = Q_w^*\rho_c g H[p' - (1 - \epsilon^*)] \quad (25)$$

The energy dissipated owing to the rising bubbles is expressed using the product of slip velocity and slip force:

$$E_b = 2\pi HR^2\left[\int_0^\delta U_s F_s\xi\, d\xi + \int_\delta^\lambda U_s^* F_s^*\xi\, d\xi\right] \quad (26)$$

It may be seen from Eqs. 1 and 2 that for each zone:

$$F_s = g\epsilon(1 - \epsilon)(\rho_c - \rho_d) \simeq g\epsilon(1 - \epsilon)\rho_c \quad \text{and} \quad F_s^* \simeq g\epsilon^*(1 - \epsilon^*)\rho_c \quad (27)$$

Slip velocity is usually taken to depend only on voidage, and according to Wallis (1969):

$$U_s = U_\infty(1 - \epsilon)^{n-1} \quad \text{or} \quad U_s^* = U_\infty^*(1 - \epsilon^*)^{n^*-1} \quad (28)$$

where U_∞ denotes single bubble rise velocity in an infinite medium. Equation 26 finally reduces to

$$E_b = \rho_c g\pi R^2 H[\delta^2 U_\infty\epsilon(1 - \epsilon)^n + (\lambda^2 - \delta^2)U_\infty^*\epsilon^*(1 - \epsilon^*)^{n^*}] \quad (29)$$

By allowing two different bubble rise velocities, which may be estimated from the Peebles-Garber relations as shown in Wallis (1969), it is possible to account for different bubble sizes. Thus, both bubble rise velocity and drift exponent may vary from zone to zone. This feature is quite new, providing considerable flexibility in forecasting behavior for practically any circumstance which might arise in two-phase flow.

The final form of the mechanical energy balance may be written:

$$p'Q_d = [\epsilon Q_c + \epsilon^* Q_w^*] + \pi R^2[\delta^2 U_\infty\epsilon(1 - \epsilon)^n + (\lambda^2 - \delta^2)U_\infty^*\epsilon^*(1 - \epsilon^*)^{n^*}] \quad (30)$$

Recent findings by Rice and Littlefield (1987) and Yang et al. (1986) seem to show that for high quality spargers, $2 < n < 3$, while Wallis (1969) suggests $0 < n < 2$. Very small bubbles behave as rigid spheres, so that $n^* = 4.45\,(Re_\infty^*)^{-0.01}$ according to Richardson and Zaki (1954).

Under certain extreme conditions when $\epsilon \to \epsilon^*(U_\infty \to U_\infty^*, n \to n^*)$, the mechanical energy balance reduces to the "ideal bubbly flow" model originally developed by Nicklin (1962):

$$\frac{U_{og}}{\epsilon} \simeq U_\infty(1 - \epsilon)^{n-1} = U_s \quad (31)$$

Table 1. Parameters used for Figure 1

			Estimated Parameters						Computed Parameters (R = 0.069 m)						
#	ν $\times 10^6$	u_{og} $\times 10^2$	ϵ' $\times 10^1$	γ $\times 10^1$	n	U_∞ $\times 10^1$	n^*	U_∞^* $\times 10^1$	ϵ $\times 10^1$	δ $\times 10^1$	α	ℓ^* $\times 10^1$	λ $\times 10^1$	p' $\times 10^1$	Q_c $\times 10^3$
1	1.00	3.80	1.17[a]	3.75[a]	1.00[f]	2.86[b]	2.80[d]	1.07[h]	1.66	7.29	0.927	0.544	9.89	8.814	1.435
2	1.00	1.90	0.74[a]	6.00[a]	3.00[g]	2.86[b]	2.40[d]	1.72[h]	0.92	7.37	0.907	0.348	9.87	9.241	1.247
3	10.0	1.00	0.50[e]	5.00	3.20[d]	2.22[c]	3.50[d]	1.11[c]	0.71	7.04	0.937	0.730	9.67	9.461	0.687
4	50.0	1.00	1.07[e]	5.00	3.90[d]	1.30[c]	4.30[d]	0.65[c]	1.53	6.85	1.054	1.900	9.61	8.846	0.414

[a]Estimated from Hills (1974), Plate *B*
[b]Estimated from Yang et al. (1986)
[c]Estimated from Rice and Littlefield (1987), d_b = 4.0 mm
[d]Estimated using Richardson-Zaki Relation (1954)
[e]Computed from drift flux with stated n and U_∞
[f]Recommended by Turner (1966) for larger bubbles
[g]Recommended by Rice and Littlefield (1987) and Yang et al. (1986)
[h]Estimated from Rice and Littlefield (1987), d_b = 2.4 mm, $d_b^* = \gamma d_b$

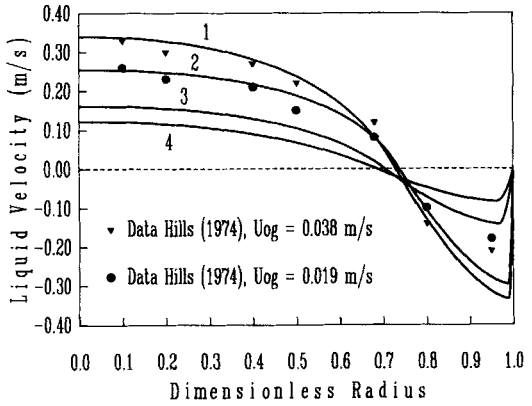

Figure 1. Velocity profile predictions for increasing viscosity: comparison with Hills' (1974) water data for plate B.
For the parameters used, refer to Table 1.

Comparison with Experiment

The above set of equations are closed to find δ, ϵ, with the specification of the gas flowrate, Q_d, and the corresponding bulk voidage, which is connected to the zone voidages through a material balance:

$$\epsilon' = \epsilon\delta^2 + \epsilon^*(\lambda^2 - \delta^2) \tag{32}$$

This third relation allows known values of ϵ' to be used to find a suitable value for α (the second von Kármán parameter).

Predicted velocity profiles are shown as curves in Figure 1 (parameters for which are in Table 1) with experimental points taken from Hills (1974). The comparison is quite good, notwithstanding the possibly large errors in velocity near the wall, where measurements are quite inaccurate.

Figure 1 also shows how the local turbulence theory predicts behavior for increasing molecular viscosity. The laminar wall layer thickens as noted by Walter and Blanch (1983), while the inversion point (δ) moves closer to the centerline.

Comments and Conclusion

By accounting for molecular viscosity in the buffer zone and wall layer, we eliminate the need for the two separate models used by Walter and Blanch (1983) and Ulbrecht et al. (1985), who allowed wall slip to occur. For low viscosity liquids such as water, the unified treatment yields a clear boundary layer of only a few millimeters, as observed by Ulbrecht et al. (1985), without resorting to the presumption of slip at the wall. Ulbrecht et al. (1985) and Rice-Littlefield (1987) observed that the velocity profile in the central core was plug shaped rather than parabolic, which the present model correctly predicts. We are presently modifying the unified model to accommodate a laminar layer thickness which follows Deissler's empirical formula.

Acknowledgment

This work was supported in part by a grant from the National Science Foundation (CBT 8513174) and an LSU Alumni Fellowship to Mr. Anderson.

Notation

b = inversion position, m
$b_t^2 = -(N_t^2/2) + \sqrt{(N_t^2/2)^2 + 1}$
cn, dn, sn = Jacobian Elliptic Functions
d_B, d_B^* = bubble diameter, m
$E(\psi, k)$ = incomplete normal elliptic integral of the second kind
E_b = rate energy dissipated from flow around bubbles, J/s
E_g = rate energy input by gas, J/s
E_v = rate energy dissipation due to velocity profiles J/s
$F(\psi, k)$ = incomplete normal elliptic integral of the first kind
F_s = slip force, N/m^3
g = acceleration due to gravity, m/s^2
$g_t = 1/(N_t^4 + 4)^{1/4}$
H = height of the emulsion, m
$k_\pm = \sqrt{1/2 \pm N_t^2/4\sqrt{(N_t^2/2)^2 + 1}}$
l^* = mixing length in buffer zone, l/R
n, n^* = drift flux exponents for core and annulus, respectively
$N_t = U_\mu/(U_t\sqrt{\lambda})$
p = pressure, kPa
p' = pressure gradient, $(-dp/dz)/\rho_c g$
Q_c = volumetric liquid flow rate in turbulent core, m^3/s
Q_d = volumetric gas flow rate, m^3/s
Q_w = volumetric liquid flow rate in clear laminar layer, m^3/s
Q_w^* = volumetric liquid flow rate in buffer zone, m^3/s
r = radial position, m
R = column radius, m
Re_∞^* = Reynolds number for small bubble, $U_\infty^* d_B^*/\nu_c$
R_c, R_c^* = Reynolds stress in core and annulus, respectively
U_c = interstitial liquid velocity in turbulent core, m/s
U_d = interstitial gas velocity, m/s
$U_t = 1/(\Gamma^* |U_{wmax}^*|)$

U_w = liquid velocity in clear laminar layer, m/s
U_w^* = interstitial liquid velocity in buffer zone, m/s
U_{og} = superficial gas velocity, m/s
U_s, U_s^* = slip velocity in core and annulus, respectively, m/s
U_∞, U_∞^* = single bubble rise velocity in core and annulus, respectively, m/s
$U_\mu = 0.5\,\nu_c/(RI^{*2}|U^*_{wmax}|)$

Greek letters

α = second von Kármán parameter
$\beta = \rho_c g R[p' - (1-\epsilon)]/2$
$\beta^* = \rho_c g R[(1-\epsilon^*) - p']/2$
γ = voidage ratio ϵ^*/ϵ
$\Gamma = \kappa\sqrt{\rho_c/\beta}$
$\Gamma^* = I^*\sqrt{\rho_c/\beta^*}$
δ = inversion point, b/R
$\epsilon, \epsilon^*, \epsilon'$ = void fractions; core, annulus, and bulk, respectively
κ = first von Kármán parameter $\simeq 0.4$
λ = "downward velocity maximum" position
μ_c = molecular viscosity of continuous phase ($\upsilon_c = \mu_c/\rho_c$), kg/ms
ξ = radial position, r/R
ρ_c, ρ_d = fluid densities, continuous and dispersed phase, respectively, kg/m^3
τ_w = shear stress in clear laminar layer
ψ = argument in elliptic integrals

Literature Cited

Byrd, P. F., and M. D. Friedman "Handbook of Elliptic Integrals for Engineers and Physicists," Lange, Maxwell, and Springer Ltd., London (1954).

Clark, N. N., C. M. Atkinson, and R. L. C. Flemmer, "Turbulent Circulation in Bubble Columns," *AIChE J.*, **33,** 515 (1987).

Hills, J. H., "Radial Non-Uniformity of Velocity and Voidage in a Bubble Column," *Trans. Inst. Chem. Engrs.*, **52,** 1 (1974).

Nicklin, D. J., "Two-Phase Bubble Flow," *Chem. Eng. Sci.*, **17,** 693 (1962).

Rice, R. G., and M. A. Littlefield, "Dispersion Coefficients for Ideal Bubbly Flow in Truly Vertical Bubble Columns," *Chem. Eng. Sci.*, **42,** 2645 (1987).

Richardson, J. F., and W. N. Zaki, "Sedimentation and Fluidisation: Part I," *Trans. Inst. Chem. Engrs.*, **32,** 35 (1954).

Rietema, K., "Science and Technology of Dispersed Two-Phase Systems—I and II," *Chem. Eng. Sci.*, **37,** 1125 (1982).

Riquarts, H. P., "Strömungsmechanische Modellierung von Blasensäuenreaktoren," *Chem. Ing. Tech.*, **54,** 770 (1982).

Turner, J. C. R., "On Bubble Flow in Liquids and Fluidized Beds," *Chem. Eng. Sci.*, **21,** 971 (1966).

Ueyama, K., and T. Miyauchi, "Properties of Recirculating Turbulent Two-Phase Flow in Gas Bubble Columns," *AIChE J.*, **25,** 258 (1979).

Ulbrecht, J. J., Y. Kawase, and K. F. Auyeung, "More On Mixing of Viscous Liquids in Bubble Columns," *Chem. Eng. Commun.*, **35,** 175 (1985).

Wallis, G. B., "One-Dimensional Two-Phase Flow," McGraw-Hill, New York, 248 (1969).

Walter, J. F., and H. W. Blanch, "Liquid Circulation Patterns and Their Effect on Gas Hold-up and Axial Mixing in Bubble Columns," *Chem. Eng. Commun.*, **19,** 243 (1983).

Yang, Z., U. Rustemeyer, R. Buchholz, and O. Ulfert, "Profile of Liquid Flow in Bubble Columns," *Chem. Eng. Commun.*, **49,** 51 (1986).

Appendix I

The volumetric flowrates in the three zones are obtained by integrating the velocity profiles. For the core, we obtain:

$$Q_c = 2\pi R^2(1-\epsilon)\int_0^\delta U_c\xi\,d\xi = \frac{(1-\epsilon)2\pi R^2}{\Gamma} \cdot \left\{\frac{\alpha^5\sqrt{3}}{2}\left[\frac{\pi}{6} - \tan^{-1}\left(\frac{2\sqrt{\delta}+\alpha}{\alpha\sqrt{3}}\right)\right] - \frac{3}{10}\delta^{5/2} - \frac{3}{4}\alpha^3\delta + \frac{\alpha^5}{4}\ln\left[\frac{\alpha^2+\alpha\sqrt{\delta}+\delta}{(\alpha-\sqrt{\delta})^2}\right]\right\} \quad \text{(A1)}$$

For the clear laminar wall layer, we get:

$$Q_w = 2\pi R^2\int_\lambda^1 U_w\xi\,d\xi = -\frac{\pi R^4\rho_c g}{8\mu_c}[1-p'][(1-\lambda^2)(1-3\lambda^2) - \lambda^4\ln\lambda^4] \quad \text{(A2)}$$

Finally, for the buffer zone, the flow rate is predicted to be:

$$Q_w^* = 2\pi R^2(1-\epsilon^*)\int_\delta^\lambda U_w^*\xi\,d\xi = \pi R^2(1-\epsilon^*)|U^*_{wmax}|\left\{-\lambda^2 - \frac{U_\mu}{3}(\lambda^3-\delta^3) - \frac{2}{7}U_\mu\lambda^3\left(\frac{N_t^2}{5}-\frac{1}{3}\right) + \frac{2}{7}U_t\sqrt{\delta}\left(\frac{2}{3}\lambda^2 + \frac{1}{5}N_t^2\lambda\delta - \delta^2\right)\sqrt{\lambda^2+N_t^2\delta\lambda-\delta^2} + \frac{2}{7}g_tU_t\lambda^{7/2}\left[\frac{2}{3}M_0(\lambda) + \frac{29}{15}N_t^2b_t^2k_+^2M_2(\lambda) + \frac{4}{5}N_t^4k_+^4b_t^4M_4(\lambda)\right] - \frac{2}{7}g_tU_t\lambda^{7/2}\left[\frac{2}{3}M_0(\delta) + \frac{29}{15}N_t^2b_t^2k_+^2M_2(\delta) + \frac{4}{5}N_t^4k_+^4b_t^4M_4(\delta)\right]\right\} \quad \text{(A3)}$$

where

$$M_0(x) = F(\psi_x, k_+) = u_x$$

$$M_2(x) = \frac{1}{k_+^2k_-^2}\left[E(\psi_x,k_+) - k_-^2F(\psi_x,k_+) - k_+^2sn(u_x)\frac{cn(u_x)}{dn(u_x)}\right]$$

$$M_4(x) = \frac{2(2k_+^2-1)M_2(x) + M_0(x) - sn^3(u_x)cn(u_x)/dn^3(u_x)}{3k_+^2k_-^2}$$

$$U^*_{wmax} = -\frac{\rho_c g R^2}{4\mu_c}[1-p'][1-\lambda^2+\lambda^2\ln\lambda^2].$$

Manuscript received Sept. 2, 1988, and revision received Nov. 8, 1988.